observed systematic absences of $h0l$ ($l = 2n+1$) and $0k0$ ($k = 2n + 1$) uniquely define the space group as $P2_1/c$. The unit cell and data collection parameters are summarized in Table VI. Throughout data collection four standard reflections from diverse regions of reciprocal space were measured every 50 reflections. The intensities of the standard reflections showed no systematic variations during data collection.

Data reduction, solution, and refinement of the structure were performed with the SHELXTL structure determination package (Nicolet XRD Corp., Madison, WI). Direct methods were used to locate the positions of the iron atoms. Subsequent difference Fourier maps revealed the location of the remaining non-hydrogen atoms. All hydrogen atoms were included as fixed contributions at idealized locations except the carbene hydrogen H(1) which was located and isotropically refined. Psi scan absorption corrections were found not to lead to any improvement in the refinement and were consequently omitted.

Some disorder in the PF_6 counterion was evident, particularly from the large thermal elipsoids of the fluorine atoms. However, difference Fourier maps failed to suggest a suitable disorder model. The final refinement converged at $R = 0.051$ and $R_w = 0.049$. The magnitude of the largest peak on the final electron density difference map was 0.54 e/Å^3.

Acknowledgment. Support from the National Science Foundation is gratefully acknowledged. We thank Professor Richard F. Fenske, Paul T. Czech, and Dr. Kenneth J. Haller for helpful discussions. M.C. thanks the Science and Engineering Research Council (U.K.) for a NATO postdoctoral fellowship. G.P.N. thanks the Wisconsin Alumni Research Foundation for a fellowship. M.S.K. thanks SOHIO for a fellowship.

Supplementary Material Available: Tables of atomic coordinates, bond distances, bond angles, and anisotropic thermal parameters (6 pages); listing of structure factors (calculated vs observed) (28 pages). Ordering information is given on any current masthead page.

IR Flash Kinetic Spectroscopy of Transients Generated by Irradiation of $(\eta^5\text{-}C_5H_5)Co(CO)_2$ in the Gas Phase and in Solution

Eric P. Wasserman, Robert G. Bergman,* and C. Bradley Moore*

Contribution from the Department of Chemistry, University of California, and the Materials and Chemical Sciences Division of the Lawrence Berkeley Laboratory, Berkeley, California 94720.
Received February 5, 1988. Revised Manuscript Received April 11, 1988

Abstract: The photoinduced ligand substitution chemistry of $(\eta^5\text{-}C_5H_5)Co(CO)_2$ in the gas and solution phases has been studied by using laser flash kinetic spectroscopy with fast IR detection. The data are consistent with primary loss of one CO to form an unsaturated species which then reacts with ligands such as C_2H_4 in the gas phase or with $P(n\text{-}C_4H_9)_3$ in cyclohexane solution. The rates of bimolecular ligand addition reactions have been measured for several ligands. In general, the unsaturated intermediate reacts with ligands at rates close to those of diffusion in both media, which indicates that the open site of the coordination sphere may be only weakly solvated in alkane solutions. Solvation complexes of this intermediate with benzene and tetrahydrofuran in cyclohexane solution were produced; these solvates are far less reactive than the cyclohexane solvate. The benzene solvate appears to react with ligand through both direct and indirect pathways. The rate constants for these reactions have been determined.

The role played by solvent molecules in organometallic reactions is not well-understood. This is especially true for nonaqueous solutions, whose physical properties have received relatively little attention, given the enormous experimental literature on the effect of solvent on the reactivity and thermodynamics of organic molecules and of simple inorganic ions.[1] It is known, however, that varying the solvent has a profound effect on the reactivity of coordinatively unsaturated organometallic species.[2] Coordination of solvent has a profound effect on the rate of carbonyl migratory insertion,[3a] one of the most well-studied organometallic transformations.[3b,c] In the case of octahedral WL_6 complexes,[3d] the presence of a solvent molecule effectively locks the pentacoordinate WL_5 photoproduct into distinguishable octahedral geometries, an interaction so strong as to lead Dobson et al. to coin the term "token ligand" for the occupant solvent molecule. The recent discovery of solvates of C-H activating fragments in ultracold matrices[4] has raised our curiosity about their role in solution-phase mechanisms, since the solvating hosts range from noble gas to potentially reactive matrices.

Within the past several years, the technique of flash photolysis, combined with fast detection of transient species, has led to significant contributions to the understanding of fundamental problems in organometallic chemistry.[5] In this work, an important unsaturated organometallic fragment, $CpCo(CO)$ ($Cp = \eta^5\text{-}C_5H_5$), is studied in both the gas and solution phases. The extent to which solvent occupation and stabilization of the open site affects its reactivity is determined for two-electron donor ligands.

$CpCo(CO)_2$ was settled on as a good starting point for our study for several reasons. A volatile (partial pressure at 300 K $\simeq$ 1.1 Torr), light-sensitive compound, it lends itself to gas- as well as liquid-phase photochemical study. Not only is it a congener of the second- and third-row C-H activating compounds $Cp^{(*)}M(CO)_2$ (M = Rh, Ir; $Cp^* = \eta^5\text{-}C_5Me_5$)[6] but $CpCo(CO)_2$ is also

(1) Some research on physical properties of nonelectrolytic solutions has been collected in *Physical Chemistry of Organic Solvent Systems*; Covington, A. K., Dickinson, T., Eds.; London: Plenum Press, 1973.

(2) See, for example: (a) Belt, S. T.; Haddleston, D. M.; Perutz, R. N.; Smith, B. P. H.; Dixon, A. J. *J. Chem. Soc., Chem. Commun.* **1987**, 1347. (b) Church, S. P.; Grevels, F.-W.; Hermann, H.; Schaffner, K. *Inorg. Chem.* **1985**, *24*, 418. (c) Church, S. P.; Grevels, F.-W.; Herrmann, H.; Kelly, J. M.; Klotzbuecher, W. E.; Schaffner, K. *J. Chem. Soc., Chem. Commun.* **1985**, 594. (d) Giordano, P. J.; Wrighton, M. S. *Inorg. Chem.* **1977**, *16*, 166.

(3) (a) Wax, M. J.; Bergman, R. G. *J. Am. Chem. Soc.* **1981**, *103*, 7028. (b) Kuhlman, E. J.; Alexander, J. J. *Coord. Chem. Rev.* **1980**, *33*, 195-225. (c) Alexander, J. J. *The Chemistry of the Metal-Carbon Bond*; Hartley, F. R., Ed.; Wiley: New York, 1985; Vol. 2, Chapter 5. (d) Dobson, G. R.; Hodges, P. M.; Healy, M. A.; Poliakoff, M.; Turner, J. J.; Firth, S.; Asali, K. J. *J. Am. Chem. Soc.* **1987**, *109*, 4218.

(4) Rest, A. J.; Whitewell, I.; Graham, W. A. G.; Hoyano, J. K.; McMaster, A. D. *J. Chem. Soc., Dalton Trans.* **1987**, 1181.

(5) For an excellent review on the progress in this area, cf.: Poliakoff, M.; Weitz, E. *Advances in Organometallic Chemistry*; Stone, F. G. A., Ed.; Academic Press: New York, 1986; Vol. 25, p 277.

(6) Hoyano, J. K.; Graham, W. A. G. *J. Am. Chem. Soc.* **1982**, *104*, 3723.

0002-7863/88/1510-6076$01.50/0

an important catalyst precursor in its own right, for example, in alkyne trimerization.[7] Certain results indicate that closely related molecules may be precursors to H_2-activating fragments.[8] Finally, due to its availability, structural simplicity, and chemical significance, the compound has been the subject of much pertinent investigation, both experimental[9] and theoretical.[10]

In 1977, Lee and Brintzinger examined the photochemistry of $CpCo(CO)_2$ in toluene and petroleum ethers at −78 °C,[11] in an attempt to identify spectroscopically the intermediates in the alkyne cotrimerization reaction. Under these conditions, they claimed to have seen the monocarbonyl CpCo(CO) (from its carbonyl stretch at 1970 cm^{-1}) as the first species formed upon photolysis. Subsequent reaction of this species yielded the dimers $Cp_2Co_2(CO)_3$ and $Cp_2Co_2(CO)_2$ or, in the presence of diphenyl alkynes, the monosubstituted carbonyl alkyne complex, CpCo(CO)(RC≡CR). These species then presumably lead into the trimerization pathway, the last via coordination of a second alkyne and isomerization to a coordinated cyclopentadienone derivative. In most catalytic schemes for the cotrimerization reaction, the CpCo moiety remains intact and acts as the template upon which the linking of the alkynes is effected. Later, this group isolated[12] two partially purifiable, sublimable materials assigned the formulas $CpCo(C_6H_6)$ and $CpCo(C_6H_6)_2$ on the basis of mass spectral data alone, which supported the hypothesis of CpCo being the catalytic unit involved in this cyclization. The former adduct reacted with 2-butyne to produce a material showing a parent ion in the mass spectrum consistent with its assignment as $CpCo(C_6(CH_3)_6)$.

While Rest and co-workers did not detect CpCo(CO) following the photolysis of $CpCo(CO)_2$ in Ar and CH_4 matrices,[13] but rather the dimer $Cp_2Co_2(\mu\text{-}CO)_2$, a later study[4] showed the monocarbonyls CpM(CO) (M = Rh, Ir) to be the direct products in the photolysis of the congeners of $CpCo(CO)_2$, $CpM(CO)_2$ (M = Rh, Ir). Effects particular to the matrix environment may be responsible for the discrepancy between the photochemistry that Rest observed as opposed to that seen by Brintzinger. For example, the cage effect which is of importance in matrix chemistry may drastically reduce the yield of monocarbonyl by making it impossible for photogenerated CO to escape from the monocarbonyl and diffuse away. In a CO matrix, η^3-$CpCo(CO)_3$ is produced upon photolysis, lending credence to the associative ligand substitution mechanism first advanced by Wojcicki and Basolo.[14] When photolysis is performed on the dicarbonyl isolated in N_2 matrices, $CpCo(CO)(N_2)$ is the major product.

We undertook the study of $CpCo(CO)_2$ chemistry from two directions with somewhat different motivations. First, we examined the compound in the gas phase mainly in order to understand its facile ligand substitution processes. While most time-resolved photochemical studies on ligand addition processes at inorganic carbonyls show CO loss to be the first step,[15] primary ligand association followed by CO loss cannot be ruled out in this case a priori because of its undeniable applicability in the thermal ligand substitution reactions of $CpCo(CO)_2$ as followed by CO exchange[14b] and in the thermal substitution chemistry of (indenyl)$Rh(CO)_2$ and related materials.[16] In repeating the photolysis of $CpCo(CO)_2$ in solution, we wished not only to ascertain whether CpCo(CO) is the primary photoproduct but also to establish the extent to which an incoming ligand molecule is impeded from attacking the open site on the organometallic fragment by one or more solvent molecules.

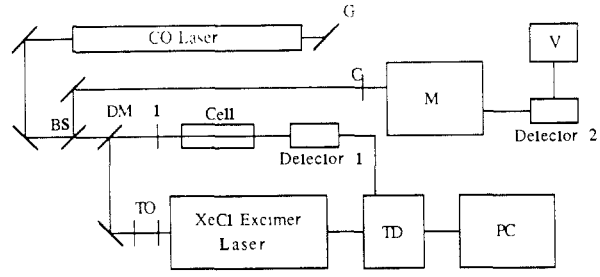

Figure 1. Schematic diagram of the transient CO laser spectrometer used for 308-nm photolysis of gas-phase samples. Abbreviations: BS, Ge beamsplitter; C, chopper; DM, dichroic mirror; G, grating; I, iris; M, 0.75 m monochromator; PC, personal computer; TD, transient digitizer; TO, telescoping optics; V, voltmeter. See Experimental Section for additional details.

Experimental Section

The apparatus used in the flash photolysis of $CpCo(CO)_2$ with CO laser detection is represented in Figure 1. The CO laser used is home-built according to the general design of Djeu[17] and is described in detail by Houston.[18] In brief, the laser is equipped with a 4.8 μm grating and is cooled by liquid nitrogen, which enables lasing action to occur from ca. 1800–2050 cm^{-1}. No feedback cavity stabilization system was used. For detection, two different detectors were employed for acquiring kinetic data (detector 1 in the diagram): a liquid nitrogen-cooled InSb photovoltaic detector and a liquid helium-cooled Ge:Cu photoconductive detector (both from Santa Barbara Research). Both detector risetimes were roughly 150 ns, while the low-frequency amplifier cutoff was about 500 Hz. The best single-shot signal-to-noise ratio on the transient absorptions would be roughly 5 for 1% change in transmitted IR light given a CO laser power of approximately 3 mW.

In each experiment, a second detector was used to monitor CO laser power. For the gas-phase experiments, a Ge beamsplitter directed half of the IR beam through a chopper wheel into a monochromator (Spex, 0.75 m, single pass, 0.1 cm^{-1} resolution) previously calibrated by the 632.8-nm line of a He:Ne laser. At the exit port of the monochromator was placed either a thermistor-cooled PbSe or a second InSb detector, from which an AC voltage proportional to laser power was obtained.

Several modifications were made to the detection system by the time the solution experiments were undertaken. The hand-tunable grating micrometer was replaced by a computer-controlled stepping motor. The stepping motor was initially calibrated against the monochromator, then the monochromator was removed from the experiment, as the reference beam was allowed to impinge directly on the reference detector (detector 2). The beamsplitter was moved directly before detector 1, so that solvent absorptions would not interfere with CO laser power normalization of the traces (see below).

For photolysis, an excimer laser (Lambda-Physik, EMG-103) was operated for XeCl* emission (308 nm). The beam, after telescoping and reflection, delivered about 5–10 mJ/cm^2·pulse over an area of 2 cm^2. When the gas cell was in use, the 308-nm photolysis beam, directed into the cell by a dichroic mirror of coated sapphire, ran coaxially with the CW CO laser beam down the center of the cell. Repetition rates for the photolysis laser ranged from 2 to 20 Hz; pulse duration was ca. 20 ns. The photolysis beam diameter, which could be altered by changing the setting of an iris placed right in front of the IR cell, ranged from 5 to 15 mm and completely contained the IR beam, whose diameter was 2–3 mm. Proper overlap of the two laser beams and maintenance of clean cell windows were crucial to the minimization of acoustic waves which could interfere in the analysis of transient signals.

The gas cell, 107-cm path length and 2.5-cm inner diameter, was equipped with two capacitance manometers for pressure measurement. Measurement of the pressure of $CpCo(CO)_2$, when necessary, was made indirectly by monitoring the amplitude of the signals due to reflections from the photolysis beam reaching two silicon photodiodes placed before and after the gas cell and applying Beer's Law, with the absorption cross section at 308 nm ($\epsilon_{10} \simeq 1400$ $l \cdot mol^{-1} \cdot cm^{-1}$). The gas mixture was slowly flowed through the cell in the following manner. The buffer gas, either He, Ar, or, for the N_2 reactions, N_2, streamed over the surface of the

(7) Vollhardt, K. P. C. *Acc. Chem. Res.* **1977**, *10(1)*, 1.
(8) Janowicz, A.; Bergman, R. G. *J. Am. Chem. Soc.* **1981**, *103*, 2488.
(9) (a) For a review, see: Basolo, F. *Coord. Chem. Rev.* **1982**, *43*, 7. (b) Vollhardt, K. P. C.; Bercaw, J. E.; Bergman, R. G. *J. Organomet. Chem.* **1975**, *97*, 283.
(10) Hofmann, P.; Padmanabhan, M. *Organometallics* **1983**, *2*, 1273.
(11) (a) Lee, W.-S.; Brintzinger, H. H. *J. Organomet. Chem.* **1977**, *127*, 87. (b) Lee, W.-S.; Brintzinger, H. H. *J. Organomet. Chem.* **1977**, *127*, 93.
(12) Lee, W.-S.; Koola, J. D.; Brintzinger, H. H. *J. Organomet. Chem.* **1981**, *206*, C4.
(13) Crichton, O.; Rest, A. J.; Taylor, D. J. *J. Chem. Soc., Dalton Trans.* **1980**, 167.
(14) (a) Wojcicki, A.; Basolo, F. *J. Inorg. Nucl. Chem.* **1961**, *17*, 77. (b) Schuster-Woldan, H.-G.; Basolo, F. *J. Am. Chem. Soc.* **1966**, *88*, 1657.
(15) Selected examples: (a) Seder, T. A.; Church, S. P.; Weitz, E. *J. Am. Chem. Soc.* **1986**, *108*, 4721. (b) Seder, T. A.; Ouderkirk, A. J.; Weitz, E. *J. Chem. Phys.* **1986**, *85*, 1977. (c) Fletcher, T. R.; Rosenfeld, R. N. *J. Am. Chem.* Soc. **1985**, *107*, 2203.
(16) Rerek, M. E.; Basolo, F. *J. Am. Chem. Soc.* **1984**, *106*, 5908.
(17) Djeu, N. *Appl. Phys.* **1973**, *23*, 309.
(18) Houston, P. L.; Moore, C. B. *J. Chem. Phys.* **1976**, *65*, 757.

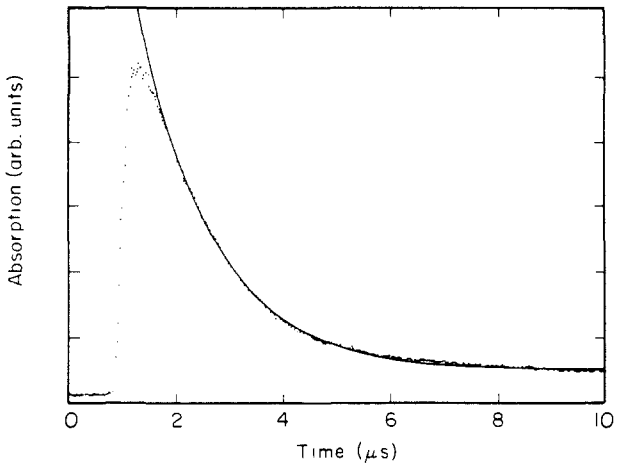

Figure 2. Transient absorption at 2011 cm^{-1} following the 308-nm photolysis of a mixture of ca. 100 mTorr $CpCo(CO)_2$ in 80 Torr Ar and an exponential fit of the decay section corresponding to k_{obsd} = (7.2 ± 0.1) × 10^5 s^{-1}.

liquid $CpCo(CO)_2$ and thence into the cell through a central port. A port at each end of the cell allowed a stream of pure buffer gas to sweep over the inner surface of the CaF_2 windows, which were placed at Brewster's angle. Typical experimental conditions were 0.3 Torr $CpCo(CO)_2$ and 50 Torr Ar. Of the gases, N_2 (99.998%), Ar (99.995%), and He (99.995%) were supplied by Lawrence Berkeley Laboratory, while the CO (99.5%) and C_2H_4 (99.5%) were from Matheson. $CpCo(CO)_2$ was vacuum distilled before being placed in the gas cell apparatus. (The material decomposed slowly while under inert gas and shielded from light, but as the decomposition products are nonvolatile clusters, no subsequent purification was deemed necessary).

For the liquid-phase experiments, a standard rectangular IR cell with CaF_2 windows (2 × 3.8 cm, one window drilled with holes top and bottom) separated by Teflon or lead gaskets of 1 or occasionally 0.5 mm thickness was used. Unless stated, solutions were purged of nitrogen by bubbling argon through them for roughly 5 minutes before use. An overpressure of Ar in a flask containing the solution forced it through Teflon delivery tubes into the cell, from which it left through more Teflon tubing. The flow rate of solution varied, but it was typically 1 $cm^3 \cdot s^{-1}$. This flow rate, given the cross section of the IR beam (ca. 0.03 cm^2) and the photolysis repetition rates used, was found to be sufficient to ensure fresh sample for each photolysis shot. Solutions were prepared in a drybox under N_2. The concentration of $CpCo(CO)_2$ was typically 0.3–1 × 10^{-3} M in cyclohexane. The cyclohexane, THF, and benzene were purchased from Fisher and were distilled from $LiAlH_4$ (C_6H_{12}) and Na/benzophenone (THF, C_6H_6). $P(n\text{-}C_4H_9)_3$ was obtained from Aldrich and was used without further purification. Acetonitrile was obtained from Merck and distilled from CaH_2. $CpCo(CO)_2$ was vacuum distilled and stored under nitrogen at reduced temperature.

The transient absorptions associated with the kinetics were digitized and averaged by a transient digitizer (Tektronix, 7912AD) which was triggered by a TTL pulse from the Synch Out of the excimer used. The transient digitizer was controlled by a Fountain-XT computer, which also could be used for data analysis. Transient spectra were assembled from the individual kinetic traces acquired at each CO laser frequency by first aligning all traces to the same base line, normalizing each trace for laser power, and displaying the relative absorption of CO laser output, positive or negative, as a function of frequency at a specified time, e.g., 5 μs, after the firing of the photolysis laser. Typically, 128 photolysis shots were used to acquire each gas-phase kinetic trace, while 16 shots were used in the solution experiments. The decaying or rising profiles of the transient absorptions were fit to first-order exponentials by using a Marquardtian nonlinear least-squares iterative fitting procedure.[19] Occasionally, e.g., for the kinetic data quoted for the reaction of CpCo(CO) with C_2H_4, a shock wave artifact had to be eliminated from the kinetic trace by subtracting a normalized trace taken at a frequency at which there were no transient absorptions from the trace at the frequency of interest.

Results and Discussion.

Gas-Phase Photolysis of $CpCo(CO)_2$. Figure 2 shows transient absorption of 2011 cm^{-1} light following the photolysis of $CpCo(CO)_2$ in buffer gas (Ar), along with a superimposed fit to a first-order exponential decay. From a collection of such transient absorption traces taken through the CO laser frequency range, we construct transient absorption spectra (see Experimental Section). Figure 3 shows the transient absorption spectra observed 1 and 3 μs after the 308-nm photolysis of $CpCo(CO)_2$ (**1**) in ca. 45 Torr of He in the presence of 1 Torr CO. The negative relative absorptions centered at 1990 and 2040 cm^{-1} are due to the prompt depletion of **1** upon photolysis. A study of the variation of the amplitude of the positive transient observed at 2010 cm^{-1}, normalized for CO laser power, with photolysis laser power over a fluence range of 0.1–1 mJ cm^{-2} $pulse^{-1}$ indicates that a one-photon process is responsible for the production of this transient. Figure 3 shows that within 3 μs, the transient at 2010 cm^{-1} disappears, while a new positive transient near 1980 cm^{-1} grows in on the same time scale. At 2030 cm^{-1}, there is a somewhat smaller positive transient which forms promptly and does not decay on the 20 μs time scale of these spectra.

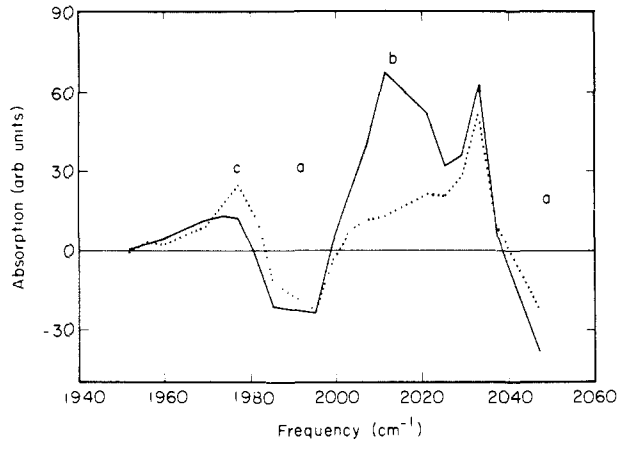

Figure 3. Transient absorption spectra from the 308-nm photolysis of $CpCo(CO)_2$ in 45 Torr He with 1 Torr CO, 1 (solid line) and 3 μs (dotted) after photolysis: a, $CpCo(CO)_2$; b, $CpCo(CO)$; c, $Cp_2Co_2(CO)_3$.

We feel confident in the identification of the 2010 cm^{-1} transient as the unsaturated species, $CpCo(CO)$ (species **2** in Scheme I, drawn with a bent structure as indicated by the calculations in ref 10). The band is unique in the spectrum, as its kinetic behavior cannot be correlated with that of any other band down to 1900 cm^{-1}. The rate of disappearance of this species, obtained from the fit of the transient absorption to an exponential decay, grows linearly with the partial pressure of CO (varied from 0 to 5 Torr), a result consistent with simple ligand addition (Scheme I). At higher CO pressures (>1 Torr), the rate at which $CpCo(CO)_2$ grows back in after photolysis is approximately that of the disappearance of the 2010-cm^{-1} transient. We have determined the residual rate of decay of the transient to be due to reaction of the monocarbonyl with starting material (see below). The product of this reaction shows a terminal CO absorption at 1980 cm^{-1}, and on this basis we postulate it to be the binuclear species $Cp_2Co_2(CO)_3$, denoted as **5**.

We have not been able to positively identify the species responsible for the transient absorption at 2030 cm^{-1}, though it is most likely monometallic, since it appears faster than does **5**, which is formed at a rate close to the rate of diffusion (see below). This feature is only seen in experiments in which CO was added. It is possible that this transient corresponds to the η^3-Cp product seen in the photolysis of $CpCo(CO)_2$ in CO matrices, $(\eta^3\text{-Cp})Co(CO)_3$, which has CO stretching vibrations at 2075 and 2018 cm^{-1}. Our CO laser range does not extend high enough in frequency to search for transient absorption at 2075 cm^{-1}, and thus this assignment remains a speculation.

This limitation also prevents us from examining the internal energy distribution of CO in low-lying vibrational states. In order to influence the reported spectra, the CO would have to be highly vibrationally excited ($v \geq 3$). We do not believe that such "hot" CO is responsible for any of the transients observed in our spectra, since the CO ejected from $Cr(CO)_6$ has been found[15c] to be

(19) Bevington, P. R. *Data Reduction and Error Analysis for the Physical Sciences*; New York: McGraw-Hill, 1969; p 232.

Scheme I

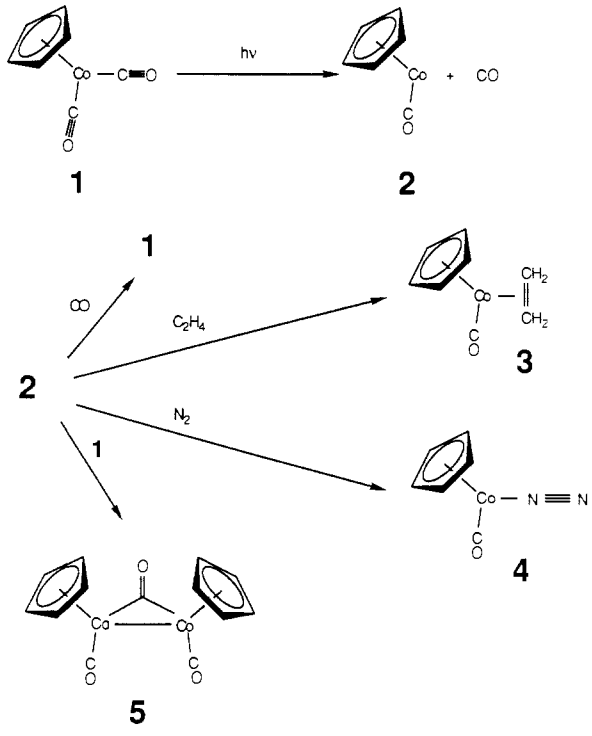

Table I. Rate Constants for the Reaction of CpCo(CO) with Various Molecules in the Gas Phase

ligand	rate constant (cm^3 $molecule^{-1}$ s^{-1})
CO (4 Torr Ar)	$(2.2 \pm 0.4) \times 10^{-11}$
CO (9 Torr Ar)	$(2.4 \pm 0.5) \times 10^{-11}$
CO (36 Torr Ar)	$(2.7 \pm 0.6) \times 10^{-11}$
CO (95 Torr Ar)	$(3.3 \pm 0.6) \times 10^{-11}$
C_2H_4	$(2.3 \pm 0.4) \times 10^{-11}$
N_2	$(1.0 \pm 0.2) \times 10^{-13}$
$CpCo(CO)_2$	$(2 \pm 1) \times 10^{-10}$

[a] Uncertainties are 95% confidence limits. To convert rate constants to units of M^{-1} s^{-1}, multiply values by 6.022×10.[20]

predominantly in the ground vibrational state. Also, the kinetic behavior of the positive transients does not correspond to that which one would predict for vibrationally excited CO.

In the gas phase, removal of energy is required during the formally bimolecular reaction CpCo(CO) + L = CpCo(CO)L, and it must be accounted for in any kinetic scheme. Since this reaction is exothermic, at least one buffer gas molecule must collide with the association complex [CpCo(CO)L]* in order to prevent the reverse reaction from occurring.[20] The amount of vibrational energy remaining in the monocarbonyl fragment after photolysis will certainly contribute as well to the number of effective collisions required to trap CpCo(CO)L as the ligand addition product. In our kinetic studies on the reactivity of the monocarbonyl, we wanted to be sure that the excess energy from the ligand addition reaction, deriving from its exothermicity, would be removed rapidly by buffer gas. To determine this, we measured the rate of reaction of **2** with CO at four different argon pressures ranging from 4 to 95 Torr (Table I). We saw a slight dependence of the rate on buffer gas pressure, but the magnitude of this effect is not much greater than that of the uncertainty in the rate determination. Our kinetic studies were all performed with 20 Torr or more of buffer gas pressure, at which pressures product trapping should be complete.

The thermalized coordinatively unsaturated species **2** (the 2010-cm^{-1} transient) reacts readily with good two-electron donors such as CO, following the pattern of $Cr(CO)_4$, $Fe(CO)_3$, and other complexes.[15] Table II shows the CO stretching absorptions we

(20) Fletcher, T. R.; Rosenfeld, R. N. *J. Am. Chem. Soc.* **1986**, *108*, 1686.

Table II. Comparison of Gas-Phase Work[a] and Relevant Matrix Studies

compound	$\tilde{\nu}$ (cm^{-1}) gas	$\tilde{\nu}$ (cm^{-1}) matrix[b]
$CpCo(CO)_2$	2045, 1985	2032.1, 1971.9
CpCo(CO)	2010	
$Cp_2Co_2(CO)_3$	1980	
$CpCo(CO)(C_2H_4)$	2005	
$CpCo(CO)(N_2)$	2005	1981.9
η^3-$CpCo(CO)_3$		2075, 2018

[a] For this work, spectral peaks can be known to within 4 cm^{-1}. [b] Reference 13.

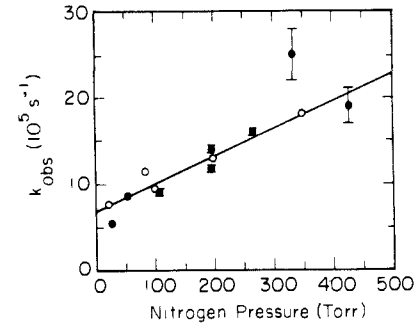

Figure 4. Dependence of the inverse of the decay time of the monocarbonyl transient upon the partial pressure of nitrogen, under both static (shaded circles) and flowing cell (open circles) conditions.

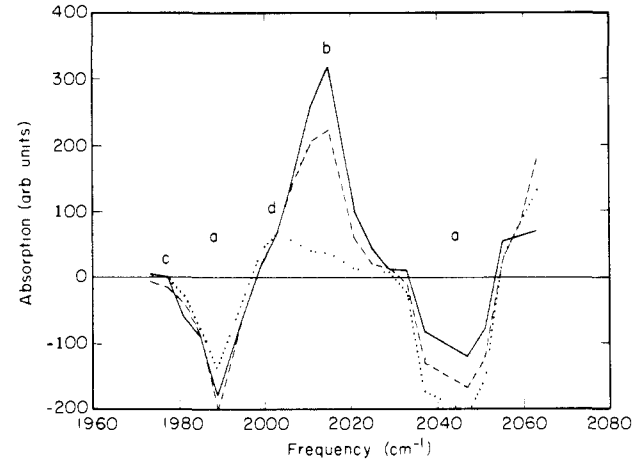

Figure 5. Transient spectra obtained 0.4 (solid line), 1.2 (dashed), and 7.6 μs (dotted) after 308-nm photolysis of $CpCo(CO)_2$ in ca. 90 Torr N_2: a, $CpCo(CO)_2$; b, CpCo(CO); c, $Cp_2Co_2(CO)_3$; d, $CpCo(CO)(N_2)$.

observe for the products formed from reaction with C_2H_4 and N_2 (species **3** and **4**, respectively) as well as those determined from matrix isolation work or other sources; the rates of reaction can be found in Table I. While CO and C_2H_4 react with the monocarbonyl at nearly the diffusion-limited rate, N_2 forms a stable complex with **2** much less readily (see Table I, Figure 4). In fact, nitrogen pressures had to be raised so high (Figure 4) to observe changes in monocarbonyl lifetime that argon gas pressure was correspondingly lowered so that total pressure was kept constant, in order to forestall large changes in the bulk properties of the sample mixture. That such a molecule is formed at all at room temperature and in the gas phase is of interest, for while the dinitrogen complex was detected in matrix studies,[13] it had not previously been seen in other media. Figure 5 shows the appearance of the dinitrogen product CO stretch at ca. 2005 cm^{-1} in a bath of pure nitrogen at ~90 Torr. Note that the CO stretch is shifted to slightly lower frequency in the dinitrogen and ethylene complexes from the monocarbonyl, indicating greater electron density on the metal center, part of which is donated into the π^* orbitals of the CO moiety.

As mentioned above, in the absence of added ligand, CpCo(CO) decays by attack on the starting complex **1**. In order to obtain

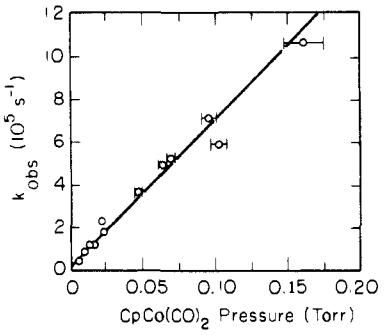

Figure 6. Dependence of the inverse of the decay time of the monocarbonyl absorption upon the partial pressure of $CpCo(CO)_2$.

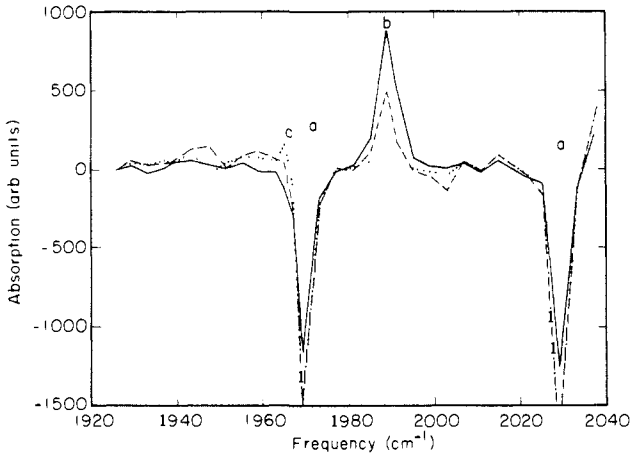

Figure 7. Transient spectra obtained 0.25 (solid line), 0.75 (dashed), and 1.5 μs (dotted) after the 308-nm photolysis of a 2.9×10^{-4} M solution of $CpCo(CO)_2$ in cyclohexane: a, $CpCo(CO)_2$; b, $CpCo(CO)$(cyclohexane); c, $Cp_2Co_2(CO)_3$.

a rate constant for this process, the partial pressure of **1** must be known. (Since rarely more than 5% of the starting material in the photolysis beam was consumed per shot, the pseudo-first-order approximation was employed.) The technique used to deliver the gaseous mixture of **1** in buffer gas into the gas cell and the flowing arrangement of the cell made it necessary to measure this quantity indirectly (see Experimental Section for details). The uncertainties involved in the conversion of UV absorption of the gas sample into **1** concentration, for example, due to the error in estimation of the true path length of the sample caused by buffer gas flow on the windows, account therefore for the greater part of the uncertainty in the rate reported for the reaction of the monocarbonyl with the unreacted dicarbonyl. The method appeared to work well, however, to the extent that the inverse lifetime of the monocarbonyl is proportional to this derived $CpCo(CO)_2$ partial pressure (Figure 6). The rate constant for this dimerization reaction as well as those for reaction with CO and C_2H_4 is close to gas kinetic. This is indicative of small barriers to reaction and is consistent with similar studies on the reactivity of $Cr(CO)_4$.[20]

Previous studies[15] of the UV photochemistry of metal carbonyls in the gas phase have shown that dissociation of more than one CO moiety is predominant. We cannot eliminate the possibility that some CpCo is formed upon photolysis of $CpCo(CO)_2$, since this fragment is not detectable with our technique. However, the fact that the transient which we assign to CpCo(CO) appears promptly after photolysis (even in the absence of added CO) indicates that it is formed from a unimolecular process, since the concentration of photoproduct CO would be too small to account for its formation by recombination. Also, the rate for the reaction of CpCo(CO) with CO (Table I) is close to gas kinetic, and the decay of CpCo(CO) absorption is accurately fit by a single exponential from the end of the photolysis pulse (within our temporal resolution). This means that no significant amount of CpCo(CO) is derived from CpCo, since the latter must first react with CO. We presume that the high number of low-frequency modes attributable to the C_5H_5 ring lowers the RRKM rate for CpCo(CO) dissociation to the point where collisions with buffer gas molecules remove enough energy to trap the monocarbonyl.

Table III. Collected CO Stretching Frequencies (in cm^{-1}) from Solution-Phase Studies[a]

compound	$\tilde{\nu}$, this work	literature
$CpCo(CO)_2$	2030, 1969	
$CpCo(CO)(C_6H_{12})$	1990	
$CpCo(CO)(C_6H_6)$	1977	
"CpCo(CO)"		1955[b]
CpCo(CO)(THF)	1952	
$CpCo(CO)(CH_3CN)$	1940	
$CpCo(CO)(C_2H_4)$		1974[c]
$CpCo(CO)(P(n\text{-}C_4H_9))$	1925	
$CpCo(CO)(P(i\text{-}Pr)_3)$		1925[d]
$Cp_2Co_2(CO)_3$	1965, 1812	1965, 1814[e]

[a] The solvent is cyclohexane unless indicated otherwise. [b] Reference 11a. Solvent: toluene. [c] Theopold, K. H.; Bergman, R. G. *J. Am. Chem. Soc.* **1983**, *105*, 464. Solvent: C_6D_6. [d] Hoffman, L.; Werner, H. *J. Organomet. Chem.* **1985**, *289*, 141. Solvent: pentane. [e] Reference 9b. Solvent: Methylcyclohexane.

Table IV. Rate Constants for the Reaction of $CpCo(CO)\cdots$Cyclohexane with Ligands

L	k'_{obsd}, M^{-1} s^{-1}
$P(n\text{-}C_4H_9)_3$	$(2.9 \pm 0.4) \times 10^9$
CH_3CN	$(5.0 \pm 0.4) \times 10^9$
$CpCo(CO)_2$[a]	$(3.6 \pm 0.7) \times 10^9$
N_2[a]	ca. 4×10^8

[a] Determined indirectly (see text).

Solution-Phase Studies. Photolysis (308 nm) of **1** in cyclohexane solution leads to the appearance of a positive transient at 1990 cm^{-1} (Figure 7). We have postulated this transient to be the monocarbonyl weakly solvated by cyclohexane. The change in medium from gas to liquid affects both the shape and frequency of the transient absorptions, making them narrower (as the wide P and R branches found in the gas phase disappear) and shifting them to lower energy by as much as 20 cm^{-1} (Table III). The monocarbonyl solvate absorption disappears as a major new absorption grows in at 1965 cm^{-1} (not readily seen in the spectrum because of its overlap with the negative transient due to starting material destruction at 1970 cm^{-1}),[21] along with a smaller absorption at 1945 cm^{-1} which has not yet been identified. The 1965-cm^{-1} absorption corresponds to the tricarbonyl dimer adduct seen in the gas phase at 1980 cm^{-1}. If the cyclohexane solvate is produced in the presence of tri-*n*-butylphosphine, a new positive transient at 1925 cm^{-1} grows in at the same rate as that of monocarbonyl decay. This species appears to be the phosphine addition product, $CpCo(CO)(P(n\text{-}Bu)_3)$, by the similarity between its CO stretching frequency and that of the triisopropylphosphine analogue (Table III). In the presence of acetonitrile, a species which absorbs at 1940 cm^{-1} is formed, which we presume to be the acetonitrile complex, $CpCo(CO)(CH_3CN)$. The dependence of the inverse of the decay time of **2** upon ligand concentration yields k_2, the bimolecular rate constant for reaction with ligand. The extreme reactivity of the alkane-solvated monocarbonyl toward these two ligands may be seen in Table IV.

Because **2** reacts so rapidly with **1** in solution, it was necessary to use dilute concentrations of **1** and, therefore, long (>0.5 mm) cell path lengths to achieve good signal-to-noise ratios. This situation led to one major problem: it became impossible to study photolysis in neat solutions of tetrahydrofuran (THF) or benzene,

(21) At the time the gas-phase experiments were done, our CO laser could not operate below 1860 cm^{-1}. Therefore, we could not probe for bridging carbonyl absorptions. In solution, we have observed an absorption at 1812 cm^{-1} which we believe to be due to the bridging CO of $Cp_2Co_2(CO)_3$, while no other transient absorptions were observed in the 1790–1825-cm^{-1} region. We speculate that the dicarbonyl dimer $Cp_2Co_2(CO)_2$, which should also absorb in this region (see ref 11a), is produced from the photolysis of the tricarbonyl dimer in previous preparative studies. Cf: Anderson, F. R.; Wrighton, M. S. *Inorg. Chem.* **1986**, *25*, 112.

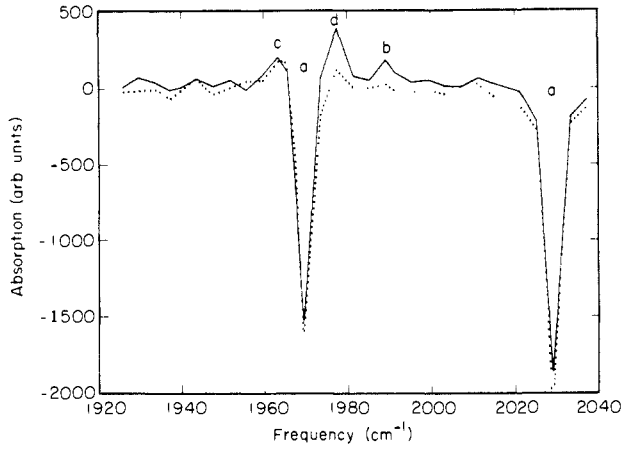

Figure 8. Transient spectra obtained 1 (solid line) and 4 μs (dotted) after the 308-nm photolysis of a 4.6×10^{-4} M solution of $CpCo(CO)_2$ in cyclohexane also containing benzene at 0.022 M concentration: a, $CpCo(CO)_2$; b, CpCo(CO)(cyclohexane); c, $Cp_2Co_2(CO)_3$; d, CpCo-(CO)(C_6H_6).

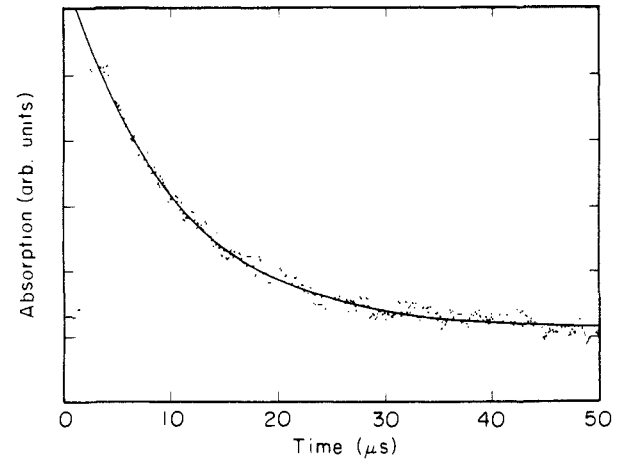

Figure 9. Transient absorption due to benzene solvate monitored at 1977 cm^{-1}. Concentrations of $CpCo(CO)_2$, C_6H_6, and $P(n\text{-}Bu)_3$ are 5.8×10^{-4}, 0.14, and 1.0×10^{-3} M, respectively. The exponential fit to the decay is overlaid; lifetime of transient is $(9.8 \pm 0.2) \times 10^4$ s^{-1}.

since in cells of this thickness these solvents either absorb all the infrared probe light or absorb enough ultraviolet photolysis light to cause solvent heating, which produces shock waves and transient changes in absorption due to changes in the refractive index and IR spectrum of the solvent. Therefore, in order to study the reactions of monocarbonyl species complexed by donor solvents, we doped cyclohexane solutions with those solvents to relatively high concentrations (ca. 0.2 M) and then varied the ligand concentration. In such cases, the kinetic scheme is more complicated, since there are two types of solvent competing for the open site on the organometallic fragment. The photolysis of **1** in one such solution doped with benzene is shown in Figure 8. The benzene solvate is formed rapidly and constitutes the major transient species present in solution after the initial photolysis pulse. A small remnant of the cyclohexane solvate is observed at 1990 cm^{-1}, while the positive transient lying at 1977 cm^{-1} represents the benzene solvate. A typical decay trace with shock-wave noise subtracted out for the benzene solvate is shown in Figure 9. The benzene solvate is most likely an η^2 side-bound species, by analogy with previously observed benzene complexes.[22] Figure 10 shows the transient spectrum of **1** photolyzed in cyclohexane solution in the presence of THF. The THF-solvated monocarbonyl appears at 1952 cm^{-1} and decreases in intensity concurrent with the rise of the 1965-cm^{-1} absorption due to dimer.

(22) For example, see: Brauer, D. J.; Krüger, C. *Inorg. Chem.* **1977**, *16*, 884.

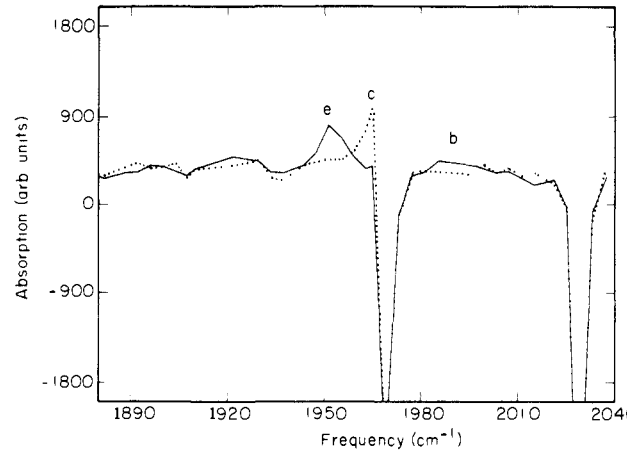

Figure 10. Transient spectra obtained 0.5 (solid line) and 2 μs (dotted) after the 308-nm photolysis of a 6.3×10^{-4} M solution of $CpCo(CO)_2$ in cyclohexane solution also containing THF at 0.012 M concentration: c, $Cp_2Co_2(CO)_3$; e, CpCo(CO)(THF). b marks the frequency at which absorption due to the cyclohexane solvate was seen previously.

Scheme II

$$CpCo(CO)_2 \xrightarrow[CyH]{h\nu} CpCo(CO)(CyH) + CO$$

$$CpCo(CO)(CyH) + S \longrightarrow CpCo(CO)(S) + CyH$$

Indirect

$$CpCo(CO)(S) + CyH \underset{k_{-1}}{\overset{k_1}{\rightleftharpoons}} CpCo(CO)(CyH) + S \qquad (K \equiv k_1/k_{-1})$$

$$CpCo(CO)(CyH) + L \xrightarrow{k_2} CpCo(CO)(L) + CyH$$

$$CpCo(CO)(CyH) + CpCo(CO)_2 \xrightarrow{k_3} Cp_2Co_2(CO)_3 + CyH$$

$$CpCo(CO)(CyH) + N_2 \xrightarrow{k_6} CpCo(CO)(N_2) + CyH$$

Direct

$$CpCo(CO)(S) + L \xrightarrow{k_4} CpCo(CO)(L) + S$$

$$CpCo(CO)(S) + CpCo(CO)_2 \xrightarrow{k_5} Cp_2Co_2(CO)_3 + S$$

$$CpCo(CO)(S) + N_2 \xrightarrow{k_7} CpCo(CO)(N_2) + S$$

(L ≡ $P(n\text{-}Bu)_3$, CH_3CN; S ≡ C_6H_6; CyH ≡ cyclohexane)

The concentration of benzene in cyclohexane was varied in order to understand the mechanism of phosphine substitution into CpCo(CO)(S), S = benzene. If the paths from donor–solvent solvate to phosphine adduct and to tricarbonyl dimer lead through an unstable unsaturated species (indirect mechanism of Scheme II), then assumption of a steady-state concentration in this unsaturated intermediate leads to the following rate law for loss of the benzene solvate

$$\text{rate} = -d[CpCo(CO)(S)]/dt = k_{obsd}[CpCo(CO)(S)] \quad (1)$$

where, at concentrations of CyH, S, L, and **1** kept high enough so that they do not change appreciably during a run

$$k_{obsd} = \frac{(k_1k_2[CyH][L] + k_1k_3[CyH][\mathbf{1}])}{(k_{-1}[S] + k_2[L] + k_3[\mathbf{1}])} \quad (2)$$

The first term in the numerator arises from the reaction of the donor–solvent solvate with ligand, while the second term represents the contribution of the dimerization reaction of the solvate with **1**; the kinetics of dimerization will be discussed later. Let us also define a quantity k'_{obsd}

$$k'_{obsd} = \frac{\partial(k_{obsd})}{\partial([L])} = \frac{k_1k_{-1}k_2[S][CyH]}{(k_{-1}[S] + k_2[L] + k_3[\mathbf{1}])^2} \quad (3)$$

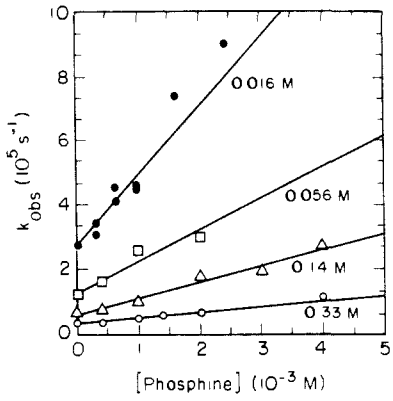

Figure 11. Dependence of the decay rate of the benzene solvate absorption upon the concentration of phosphine at four different benzene concentrations. The slopes are the effective rate constants for the reaction of the benzene solvate with phosphine.

Table V. Rate Constants for the Reaction of $CpCo(CO)\cdots C_6H_6$ with $P(n\text{-}C_4H_9)_3$ and Values of the Intercepts Taken from Their Determination

[S], M	[1], 10^{-4} M	k'_{obsd}, 10^7 M^{-1} s^{-1}	intercept, 10^5 s^{-1}
0.0078	8.1	41 ± 17	8 ± 2
0.016	5.3	22 ± 4	2.7 ± 0.1
0.056	6.2	10 ± 4	1.2 ± 0.2
0.14	5.8	5.1 ± 1.1	0.55 ± 0.11
0.22	6.0	3.4 ± 0.2	0.45 ± 0.04
0.33	4.6	1.74 ± 0.05	0.31 ± 0.07
0.53	5.9	1.8 ± 0.5	0.26 ± 0.06

which will become useful in later discussion.

Should the direct mechanism for ligand attack hold, however, the observed pseudo-first-order rate constant, k_{obsd}, would only be dependent upon the concentrations of L and **1**. If we assume that there will be components of both direct and indirect mechanisms for benzene solvate decay, then (2) and (3) become

$$k_{obsd} = \frac{(k_1k_2[CyH][L] + k_1k_3[CyH][\mathbf{1}])}{(k_{-1}[S] + k_2[L] + k_3[\mathbf{1}])} + k_4[L] + k_5[\mathbf{1}] \quad (4)$$

$$k'_{obsd} = \frac{k_1k_{-1}k_2[S][CyH]}{(k_{-1}[S] + k_2[L] + k_3[\mathbf{1}])^2} + k_4 \quad (5)$$

At each different benzene concentration, the pseudo-first-order rate constants for decay of the solvate in the presence of increasing amounts of phosphine were measured, and some of the results are shown in Figure 11. It is clear that the slopes of these lines, which represent values of k'_{obsd}, decrease with increasing [benzene]; the values of these slopes can be seen in Table V. This fact in itself is indicative of an indirect mechanism for the destruction of **6**. Also, note for Figure 11 that at no concentration of donor solvent was there significant curvature, which could indicate saturation kinetics, in the reciprocal lifetime versus ligand concentration plot. This strongly suggests that, given the expression for k_{obsd} in (4), $k_2[L] \ll (k_{-1}[S] + k_3[\mathbf{1}])$. There appears to be a linear relationship between $1/k'_{obsd}$ for benzene solvate destruction and [benzene] (Figure 12) which has an intercept at the origin. From this fact and an examination of (5), we conclude that $k_{-1}[S]$ is the dominant term in the denominator of (2) under the conditions of this experiment and also that k_4 is small, so that (4) and (5) reduce to

$$k_{obsd} = (k_1k_2[CyH][L] + k_1k_3[CyH][\mathbf{1}])/k_{-1}[S] + k_5[\mathbf{1}] \quad (6)$$

$$k'_{obsd} = k_2K[CyH]/[S] \quad (7)$$

Equation 7 illustrates the inverse dependence of the slopes of k_{obsd} versus [L] plots upon [S], the effect seen in Figure 12. From the inverse slope in Figure 12, we find $k_2K = (7 \pm 1) \times 10^5$ M^{-1} s^{-1}.

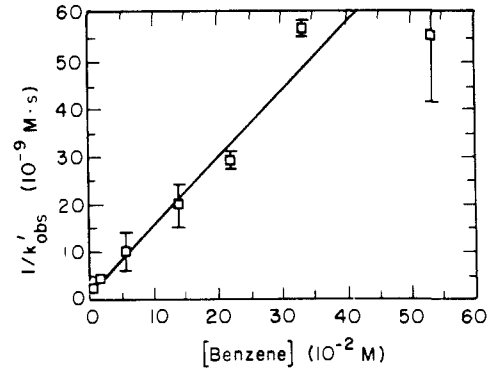

Figure 12. Dependence of the inverse of the effective rate constant for decay of the benzene solvate in the presence of phosphine upon benzene concentration.

We have already determined k_2 independently for phosphine (Table IV). If we assume the intermediate in the decay of the benzene solvate is the same cyclohexane solvate as that which reacts with phosphine in the absence of benzene, then $K = (2.3 \pm 0.5) \times 10^{-4}$.

Three points should be made here. First, the term "cyclohexane solvate" used to refer to the reactive intermediate in this Discussion does not imply a detailed knowledge of the structure or even the exact stoichiometry of this species. In fact, the degree of bonding of cyclohexane molecule(s) in the transition state between the "cyclohexane solvate" and the ligand-substituted adduct remains undetermined. Second, the fact that no saturation in the rate was observed as phosphine concentration was increased implies that k_{-1} is at least of the same order of magnitude as k_2 and is possibly even larger, since even at the highest [L]/[S] ratios (about 0.2) no significant falling off in rate was seen. This reflects the highly reactive nature of the unsaturated metal center, which reacts with any two-electron donor at about the rate of diffusion. Attempts to check this by measuring k_{-1} independently were unsuccessful, partly because the reaction of the donor–solvent solvates with **1** precluded any significant buildup of these solvates at very low concentrations of S. Finally, we must admit the possibility of a competing direct bimolecular reaction between ligand and donor–solvent solvate which might prove important at very high donor–solvent concentrations. If this were true for the case of benzene as donor solvent, then we would expect to see a leveling off of $1/k'_{obsd}$ as [S] increases. It is clear from Figure 12 that $1/k'_{obsd}$ is at least 6×10^{-8} M·s in the limit of very large [S], and thus we can derive an upper bound for k_4 of 1.7×10^7 M^{-1} s^{-1}.

The following kinetic analysis was applied to the benzene solvate decay data in order to extract the rate constant for reaction of the cyclohexane solvate with the starting material, $CpCo(CO)_2$. The decay of the benzene-solvated monocarbonyl in the absence of ligand was assumed to be entirely due to this process. From our analysis of the kinetics of reaction with ligand, $k_{-1}[S] \gg k_3[\mathbf{1}]$; so from (4), the intercept of the line through each plot of the inverse lifetime of the benzene solvate versus phosphine concentration (see Figure 11) then represents $k_3[\mathbf{1}]k[CyH]/[S] + k_5[\mathbf{1}]$; the values of these intercepts are shown in Table V. If we then plot $k_{obsd}/[\mathbf{1}]$ against $1/[S]$, we should obtain a straight line whose slope is $k_3K[CyH]$ and whose intercept at $1/[S] = 0$ is k_5. The validity of our assumptions is supported by the linearity of this plot (Figure 13), which gives $k_3 = (3.6 \pm 0.7) \times 10^9$ M^{-1} s^{-1} and $k_5 = (3.8 \pm 0.6) \times 10^7$ M^{-1} s^{-1}.

If argon is not bubbled through the solutions prior to their use in the experiments, a long-lived ($\tau > 10^{-4}$ s) absorption at ca. 1980 cm^{-1} is oberved which forms apparently within the risetime of the detector and at the expense of the monocarbonyl. This transient we believe to be the dinitrogen adduct, corresponding to the species seen in the gas phase at 2005 cm^{-1}, since the solutions were prepared under a nitrogen atmosphere.

Figure 14 shows transient absorption traces taken at 1977 cm^{-1} with two solutions which had not been purged of nitrogen and had identical benzene and $CpCo(CO)_2$ concentrations. No phosphine

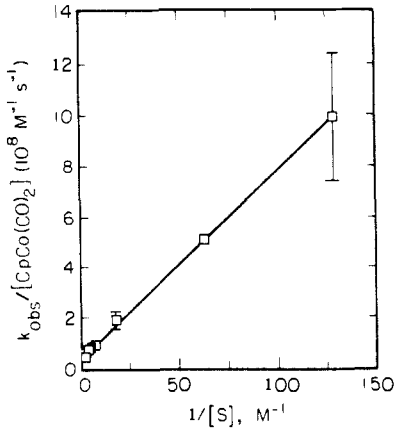

Figure 13. Dependence of $k_{obsd}/[CpCo(CO)_2]$ upon $1/[C_6H_6]$.

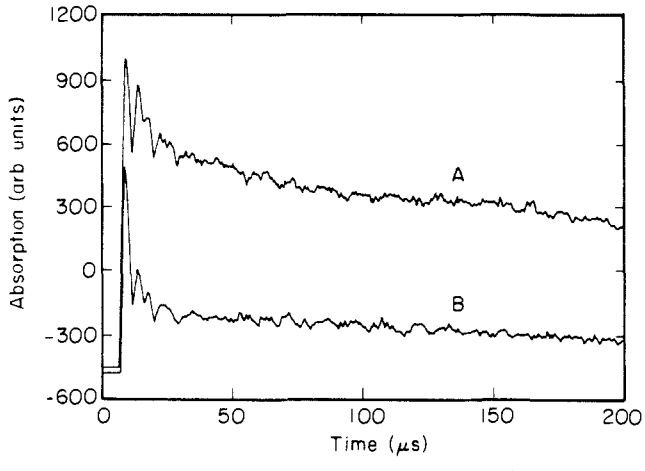

Figure 14. Transient absorption traces taken at 1977 cm^{-1} from solutions saturated with N_2. The initial oscillations in the transient absorptions are due to acoustic waves. A, that from a solution containing no phosphine; B, that from a solution containing 4.0×10^{-3} M phosphine. The concentrations of $CpCo(CO)_2$ and benzene were 5.4×10^{-4} M and 0.11 M, respectively; the power of the CO laser for trace A versus that for trace B: 1.0:1.3.

was added to the first solution, whereas its concentration in the second was 4.0×10^{-3} M. At this frequency, both the benzene and nitrogen adducts can be monitored, whereas at 1973 and 1981 cm^{-1} only the benzene solvate and the nitrogen adduct, respectively, absorb. The benzene solvate can be seen in both traces as a fast early spike, while the nitrogen adduct appears as a large base-line offset, since its decay time is much greater. It is interesting to note that the increase in phosphine concentration appears to affect the yield of nitrogen adduct and not appreciably its rate of decay, for this implies that the adduct is relatively stable to ligand attack and is more stable than the benzene solvate.

If we add reactions of nitrogen with both cyclohexane and benzene solvates (Scheme II), then the expression for the observed rate constant for benzene solvate loss is

$$k_{obsd} = \left\{\frac{k_1[CyH](k_2[L] + k_3[1] + k_6[N_2])}{k_{-1}[S] + k_2[L] + k_3[1] + k_6[N_2]}\right\} + k_4[L] + k_5[1] + k_7[N_2] \quad (8)$$

If the benzene solvate decay rate is then plotted against the concentration of phosphine, the intercept of the line through the data at [phosphine] = 0 M should be as follows

$$k_{obsd}([L] = 0) = \frac{(k_1k_3[CyH][1] + k_1k_6[CyH][N_2])}{(k_{-1}[S] + k_3[1] + k_6[N_2])} + k_5[1] + k_7[N_2] \quad (9)$$

We then made the assumption that $k_{-1}[S] \gg (k_3[1] + k_6[N_2])$, based on our experiments with phosphine. Thus

$$k_{obsd}([L] = 0) = (K[CyH]/[S])(k_3[1] + k_6[N_2]) + k_5[1] + k_7[N_2] \quad (10)$$

We estimate the nitrogen concentration in cyclohexane at 293 K to be 7.0×10^{-3} M.[23] By comparing values of $k_{obsd}([L] = 0)$ obtained at [S] = 0.11 M and at [S] = 0.022 M, we find the contribution of $k_7[N_2]$ to be negligible; $k_7 < 10^7$ M^{-1} s^{-1}. A rough value of $k_6 = 4 \times 10^8$ M^{-1} s^{-1} is obtained. A similar estimate for k_6 is obtained from the decrease in N_2 adduct formed upon addition of phosphine (from Figure 14).

Conclusions

By comparing the reactivity of the photoproducts of $CpCo(CO)_2$ produced in gas and solution phases, we have attempted to bridge the gap between the gas-phase-based and solution-based knowledge of organometallic photochemistry. CpCo(CO), whether naked (as in the gas phase) or weakly complexed by alkane, is an extremely reactive species which can be trapped by two-electron donor ligands. The liquid-phase reaction of the cyclohexane solvate with nitrogen is somewhat slower than that for reaction with phosphine or acetonitrile. This is similar to the pattern seen in the gas phase, although in the latter medium this effect is more marked. Also, we note that the dimerization reaction is nearly the fastest bimolecular process observed in both media. The reactivity of CpCo(CO)(CyH) seems in general to be high in comparison with other complexes recently studied, such as $CpMn(CO)_2(S)$[24] and $W(CO)_4(L)(S)$[3], where S represents an alkane solvent molecule.

The fact that the rate constant for direct reaction of the benzene solvate with **1** is greater than that for its reaction with phosphine is particularly intriguing and is demonstrative of the high Lewis basicity of **1**. It also raises the following question: why are dimerization reactions not more important in preparative synthetic procedures in which the concentrations of organometallic precursor and reactant ligand are similar? While the answer to this question is dependent on the exact chemical system and reaction conditions and is therefore entirely outside the scope of this article, we suggest that the instability of the initially formed dimers, such as $Cp_2Co_2(CO)_3$, in the presence of ligands over time leads indirectly to the production of ligand substitution products.

The solution-phase studies render insight into questions of solvent participation in ligand substitution, since they begin to quantify the differences in solvent-open-site bonding among solvent types. Along these lines, Wrighton and co-workers have recently observed large variations in the reactivity of unsaturated organometallic species in low-temperature hydrocarbon solvents.[25] Our studies have shown that the equilibrium constant for donor solvent versus cyclohexane solvation strongly favors benzene association at 293 K. In fact, we may crudely estimate that the metal–solvent bond of the benzene solvate is 5 kcal·mol^{-1} stronger, respectively, than that of the cyclohexane solvate. The dominance of the indirect, dissociative pathway for benzene solvate decay is in keeping with the reactivity observed by Dobson and coworkers[26] for the *cis*-(pip)(L)$W(CO)_4$ system, in which there exists a similar equilibrium between chlorobenzene and cyclohexane solvation of $(L)W(CO)_4$. Further work is planned to determine accurately the temperature dependence of these equilibria of solvate dissociation and hence the bond enthalpies of the solvent-site interaction.

Acknowledgment. We thank M. B. Sponsler, W. A. G. Graham, T. R. Fletcher, and R. N. Rosenfeld for helpful comments. The assistance of P. O. Stoutland in some of the work is gratefully

(23) Dymond, J. H. *J. Phys. Chem.* **1967**, *71*, 1829.
(24) Creaven, B. S.; Dixon, A. J.; Kelly, J. M.; Long, C.; Poliakoff, M. *Organometallics* **1987**, *6*, 2600.
(25) Hill, R. H.; Wrighton, M. S. *Organometallics* **1987**, *6*, 632.
(26) Asali, K. J.; Basson, S. S.; Tucker, J. S.; Hester, B. C.; Cortes, J. E.; Awad, H. H.; Dobson, G. R. *J. Am. Chem. Soc.* **1987**, *109*, 5386.

noted. This research was supported by the Director, Office of Energy Research, Office of Basic Energy Sciences, Chemical Sciences Division of the U.S. Department of Energy under Contract no. DE-AC03-76SF00098. C.B.M. thanks the Miller Institute for Basic Research in Science at the University of California, Berkeley, for a Research Professorship (1987-88); E.P.W. acknowledges a predoctoral fellowship from the National Science Foundation.

Registry No. 1, 12078-25-0; **2**, 73740-50-8; **3**, 77674-12-5; **4**, 73740-48-4; **5**, 53450-14-9; $CpCo(CO)(C_4H)$, 115462-20-9; $CpCo(CO)(\eta^2-C_6H_6)$, 115462-21-0; $CpCo(CO)(THF)$, 115462-22-1; $CpCo(CO)(CH_3CN)$, 115462-23-2; $CpCo(CO)(P(n\text{-}Bu)_3)$, 87145-23-1; $P(n\text{-}Bu)_3$, 603-35-0; CH_3CN, 75-05-8; N_2, 7727-37-9; CO, 630-08-0; C_2H_4, 74-85-1.

Ground Spin State Variability in $[Fe_4S_4(SR)_4]^{3-}$. Synthetic Analogues of the Reduced Clusters in Ferredoxins and Other Iron-Sulfur Proteins: Cases of Extreme Sensitivity of Electronic State and Structure to Extrinsic Factors

M. J. Carney,[1a] G. C. Papaefthymiou,[1b] K. Spartalian,[1c] R. B. Frankel,[1b,d] and R. H. Holm*,[1a]

Contribution from the Department of Chemistry, Harvard University, Cambridge, Massachusetts 02138, and the Francis Bitter National Magnet Laboratory, Massachusetts Institute of Technology, Cambridge, Massachusetts 02139.
Received February 29, 1988

Abstract: A discovery of considerable significance in the field of synthetic and biological iron-sulfur clusters is the existence of ground states of different spin multiplicities for reduced tetranuclear clusters containing the $[4Fe\text{-}4S/Se]^+$ core. In addition to the conventional $S = {}^1/_2$ ground state, states with $S = {}^3/_2$, ${}^5/_2$, and ${}^7/_2$ have been identified in proteins and enzymes. We have recently demonstrated the existence of the $S = {}^3/_2$ state in completely characterized compounds containing $[Fe_4S_4(SR)_4]^{3-}$ as the synthetic analogue of native clusters. In this work the electronic properties of some 16 compounds containing 13 different clusters have been examined by Mössbauer and EPR spectroscopy and by determination of magnetization behavior and magnetic susceptibilities. Three categories of ground spin state behavior have been identified: (i) pure spin $S = {}^1/_2$ or ${}^3/_2$; (ii) physical mixtures of $S = {}^1/_2$ and ${}^3/_2$ states; and (iii) spin-admixed ground states ($S = {}^1/_2 + {}^3/_2$). Category (i) is recognized by Curie behavior and saturation magnetization at low temperatures and by characteristic magnetic Mössbauer and EPR spectra. Of all compounds examined, only one is a pure $S = {}^1/_2$ cluster; this spin state appears to be common in proteins. Category (ii) clusters exhibit intermediate Curie constants and saturation magnetization values and composite EPR and Mössbauer spectra. Category (iii) clusters are primarily distinguished by the absence of EPR and Mössbauer features from $S = {}^1/_2$ and ${}^3/_2$ clusters. Synthetic and native clusters show substantial similarities in a given spin state; the properties of the former, which are unambiguously characterized, fully support spin state assignments of the latter. Regardless of their occurrence in these categories, all polycrystalline cluster compounds when dissolved and frozen in DMF or acetonitrile exist as physical mixtures of $S = {}^1/_2$ and ${}^3/_2$ spin states. No biological example of a spin-admixed cluster has yet been identified. It is shown that the fine details of cluster structure and accompanying stabilization of a ground spin state are highly sensitive to environment. The structures of all $[Fe_4S_4(SR)_4]^{3-}$ clusters, which show a variety of distortions from idealized cubic symmetry, are summarized and spin state-structure correlations are explored. It is concluded that, at least from structures determined at room temperature, there is no strong relationship between core structure or terminal ligand conformation and spin state. The collective results make entirely clear, by means of its responsiveness to exogenous factors, the stereochemical "softness" of the core structure which, for both synthetic and native clusters and in conjunction with ligand conformation, is doubtless of importance in stabilizing different ground spin states.

Ongoing research in this laboratory[2-12] has demonstrated that the reduced synthetic clusters $[Fe_4S_4(SR)_4]^{3-}$ manifest a structural and spin-state variability that has no parallel in the chemistry of the oxidized clusters $[Fe_4S_4(SR)_4]^{2-}$. These di- and trianionic clusters possess the cubane-type core units $[4Fe\text{-}4S]^{2+}$ and $[4Fe\text{-}4S]^+$, respectively, which are isoelectronic with cluster cores in oxidized and reduced ferredoxins (Fd) and other iron-sulfur proteins. In particular, we have recently shown that some of these reduced clusters exist in different spin ground states, $S = {}^1/_2$[11] or ${}^3/_2$,[11,12] which are exclusively occupied at very low temperatures.

It is becoming increasingly clear that biological clusters at the $[4Fe\text{-}4S]^+$ oxidation level can also deviate from what has long

(1) (a) Harvard University. (b) Massachusetts Institute of Technology. (c) Department of Physics, University of Vermont. (d) Current address: Department of Physics, California Polytechnic State University, San Luis Obispo, CA 93407.
(2) Berg, J. M.; Holm, R. H. In *Metals Ions in Biology*; Spiro, T. G., Ed.; Interscience: New York, 1982; Vol. 4, Chapter 1.
(3) Cambray, J.; Lane, R. W.; Wedd, A. G.; Johnson, R. W.; Holm, R. H. *Inorg. Chem.* **1977**, *16*, 2656.
(4) Reynolds, J. G.; Laskowski, E. J.; Holm, R. H. *J. Am. Chem. Soc.* **1978**, *100*, 5315.
(5) Laskowski, E. J.; Frankel, R. B.; Gillum, W. O.; Papaefthymiou, G. C.; Renaud, J.; Ibers, J. A.; Holm, R. H. *J. Am. Chem. Soc.* **1978**, *100*, 5322.
(6) Berg, J. M.; Hodgson, K. O.; Holm, R. H. *J. Am. Chem. Soc.* **1979**, *101*, 4586.
(7) Laskowski, E. J.; Reynolds, J. G.; Frankel, R. B.; Foner, S.; Papethymiou, G. C.; Holm, R. H. *J. Am. Chem. Soc.* **1979**, *101*, 6562.
(8) Reynolds, J. G.; Coyle, C. L.; Holm, R. H. *J. Am. Chem. Soc.* **1980**, *102*, 4350.
(9) Stephan, D. W.; Papefthymiou, G. C.; Frankel, R. B.; Holm, R. H. *Inorg. Chem.* **1983**, *22*, 1550.
(10) Hagen, K. S.; Watson, A. D.; Holm, R. H. *Inorg. Chem.* **1984**, *23*, 2984.
(11) Carney, M. J.; Holm, R. H.; Papaefthymiou, G. C.; Frankel, R. B. *J. Am. Chem. Soc.* **1986**, *108*, 3519.
(12) Carney, M. J.; Papaefthymiou, G. C.; Whitener, M. A.; Spartalian, K.; Frankel, R. B.; Holm, R. H. *Inorg. Chem.* **1988**, *27*, 346.

0002-7863/88/1510-6084$01.50/0